Herzig, P.M., Humphris, S.E., Miller, D.J., and Zierenberg, R.A. (Eds.), 1998
Proceedings of the Ocean Drilling Program, Scientific Results, Vol. 158

5. DETAILED SULFUR-ISOTOPE INVESTIGATION OF THE TAG HYDROTHERMAL MOUND AND STOCKWORK ZONE, 26°N, MID-ATLANTIC RIDGE[1]

J. Bruce Gemmell[2] and Robina Sharpe[2]

ABSTRACT

Drilling of the Trans-Atlantic Geotraverse (TAG) hydrothermal mound and underlying stockwork zone has revealed a complex internal stratigraphy consisting of, with increasing depth, massive pyrite and pyrite breccias, with significant chalcopyrite and sphalerite in places, pyrite-anhydrite breccias, pyrite-silica breccias, silicified wallrock breccias, and chloritized basalt breccias. Several stages of quartz pyrite ± chalcopyrite veins occur in the stockwork zone and lower portions of the mound whereas anhydrite ± pyrite ± chalcopyrite veins are common within the central and upper parts of the mound.

A detailed sulfur-isotope investigation of sulfides and sulfates within mound and the underlying stockwork zone has revealed that the overall range of sulfide $\delta^{34}S$ analyses is from 0.35‰ to 10.27‰, with a mean of 7.20‰. Anhydrite has a mean $\delta^{34}S$ value of 21.10‰ within a tight range of 20.55‰–21.56‰.There are distinct differences in $\delta^{34}S$ values between the different textural types of pyrite (massive sulfide, breccia clasts, disseminations associated with alteration, and veins) within the hydrothermal mound and stockwork zone. The massive sulfide and breccia clasts have a similar distribution of isotope values ($\delta^{34}S$ = 6‰–8‰), however the $\delta^{34}S$ values of the disseminated pyrite associated with the alteration are distinctly heavier ($\delta^{34}S$ = 8‰–10‰). Vein sulfides have the lightest $\delta^{34}S$ values ($\delta^{34}S$ = 5‰–7‰) at TAG. The sulfur-isotope values measured at TAG are, in general, the heaviest reported for unsedimented mid-ocean ridge deposits.

A sulfur-isotope model is proposed to account for the heavy $\delta^{34}S$ signature (compared to other sediment-free hydrothermal systems), the distribution of $\delta^{34}S$ values from the various textural styles and the spatial distribution of the $\delta^{34}S$ values both laterally and vertically throughout the hydrothermal mound and underlying stockwork zone. The two initial sources of sulfur during the life of the TAG hydrothermal system are seawater sulfate ($\delta^{34}S$ = 21‰) and mid-ocean ridge basalt (MORB) derived sulfur ($\delta^{34}S$ = 0‰–1‰). Variations in $\delta^{34}S$ values at TAG can be explained in a model where totally to partially reduced seawater sulfate of shallow origin mixes with a deep hydrothermal fluid dominated by MORB sulfur and interacts with previously formed sulfide and sulfate minerals in the upper parts of the stockwork zone and within the mound. Deep subseafloor processes cause the initial hydrothermal fluids entering the TAG system at depth to have a $\delta^{34}S$ value of approximately 0‰–1‰. This fluid mixes with locally entrained partially reduced seawater in the upper parts of the subseafloor stockwork system (created by local hydrothermal convection though the porous and permeable mound and stockwork zone) and creates a modified hydrothermal fluid with a $\delta^{34}S$ value of approximately 6‰–7‰. The fluid rises to the seafloor, precipitating pyrite in the quartz-pyrite veins ($\delta^{34}S$ = 6‰–7‰) in the upper parts of the stockwork, and mixes with cold seawater, which causes rapid precipitation of the massive pyrite ± chalcopyrite ($\delta^{34}S$ = 6‰–8‰) found at the top of the mound. Anhydrite ($\delta^{34}S$ = 20‰–21‰) is formed from the heating of entrained seawater circulating within the massive sulfide or upper parts of the stockwork zone. During periods of little or no high-temperature hydrothermal upflow, thermal collapse is accompanied by infiltration of cold seawater through the TAG mound and upper parts of the stockwork. Anhydrite that was within the mound and overlying chimneys dissolves creating clasts and fragments of pyrite ± chalcopyrite ± sphalerite within and on top of the mound. When the hydrothermal system resumes high-temperature upflow, similar processes as those described above in the initial high-temperature phase take place, precipitating massive pyrite ± chalcopyrite massive sulfide_($\delta^{34}S$ = 6‰–8‰) present at the top of the mound and the pyrite and quartz veins in the stockwork zone (vein Stages 2–4) and anhydrite ± pyrite ± chalcopyrite veins (Stage 5) within the mound ($\delta^{34}S$ = 5‰–7‰). Anhydrite in these veins, primarily Stage 5, has $\delta^{34}S$ values of 21‰, which reflects rapid heating of entrained seawater that is infiltrating the mound. Hydrothermal fluid leaks out from the veins though the porous and permeable mound and reacts with previously formed sulfides and sulfates causing the hydrothermal fluid to become slightly enriched in $\delta^{34}S$. This fluid is responsible for precipitation of disseminated pyrite, the heaviest sulfur-isotope values in the TAG system ($\delta^{34}S$ = 8‰–10‰), associated with alteration in the stockwork zone and lower portions of the mound.

INTRODUCTION

The Trans-Atlantic Geotraverse (TAG) mound is a large tonnage (approximately 4 metric tonnes), low-grade (Cu-Zn) volcanic-hosted massive sulfide (VHMS) deposit located at 26°N on the Mid-Atlantic Ridge (Fig. 1). Recent Ocean Drilling Program (ODP) coring at TAG (Humphris, Herzig, Miller, et al., 1996; Humphris et al., 1995) offers an ideal opportunity for a detailed sulfur-isotope study of a modern, seafloor volcanic-hosted massive sulfide hydrothermal system. This paper describes the sulfur-isotope characteristics of the massive sulfide mineralization, stringer veins, and alteration sulfides, and proposes a model for the sulfur-isotope systematics of an actively forming volcanic-hosted massive deposit in a sediment-free mid-ocean ridge environment. The approach used in this study is similar to the one used by Gemmell and Large (1992, 1993) in investigating the $\delta^{34}S$ characteristics of the Hellyer volcanic-hosted massive sulfide deposit in Tasmania, Australia.

Previous investigations have described various aspects of the TAG hydrothermal field: discovery (Rona et al., 1975, 1984; Thompson et al., 1985), geology (Rona et al., 1993), hydrothermal precipitates and fluid chemistry (Tivey et al., 1995; Mills, 1995), and mineralogy of the primary (Hannington et al., 1995) and secondary (Hannington et al., 1988; Hannington, 1993) mineral phases of hydrothermal precipitates. The only previous sulfide $\delta^{34}S$ values reported from TAG were included in a paper by Lein et al. (1993).

[1]Herzig, P.M., Humphris, S.E., Miller, D.J., and Zierenberg, R.A. (Eds.), 1998. *Proc. ODP, Sci. Results*, 158: College Station, TX (Ocean Drilling Program).

[2]Centre for Ore Deposit Research, University of Tasmania, GPO Box 252-79, Hobart, Tasmania 7001, Australia. bruce.gemmell@utas.edu.au

Prior Chapter Contents Next Chapter

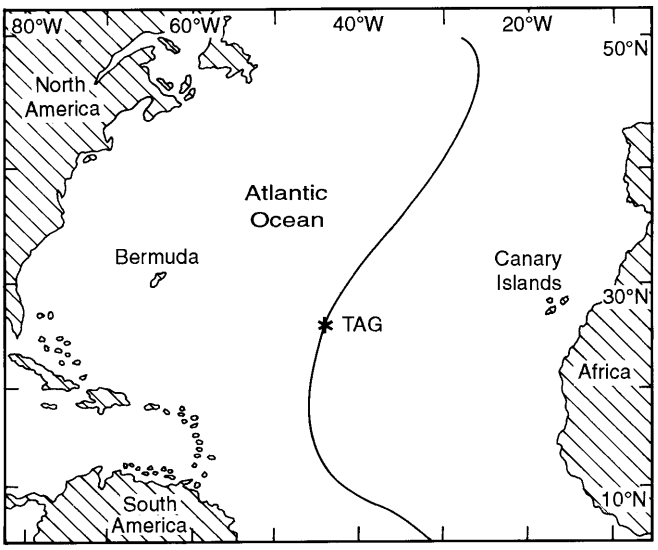

Figure 1. Location of TAG hydrothermal field at 26°N on the Mid-Atlantic Ridge.

GEOLOGY OF THE TAG DEPOSIT

The TAG hydrothermal field is the site of large active and relict sulfide deposits in the rift valley and eastern wall of the slow-spreading Mid-Atlantic Ridge at 26°N (Fig. 1). The first discovery of hydrothermal activity at TAG was by the NOAA Trans-Atlantic Geotraverse project in 1972-73, which found low-temperature hydrothermal activity and Fe-Mn oxide mineralization on the eastern wall of the rift valley (Rona et al., 1975; Rona et al., 1984; Thompson et al., 1985). The active TAG sulfide mound was discovered in 1985 and is located at a water depth of 3650 m at the base of the eastern wall of the Mid-Atlantic Ridge (Rona et al., 1993). The mound is distinctly circular, measures 200 m in diameter, rises approximately 50 m above the seafloor, and is the largest, single sulfide mound yet discovered on the seafloor (Rona et al., 1993). A cluster of black smoker chimneys emitting fluids of up to 360°C and consisting of chalcopyrite, pyrite, and anhydrite is located northwest of the center of the mound on the top of a 10–15-m-high cone (Fig. 2). A field of sphalerite-dominated white smokers venting fluids from 260° to 300°C is located in the southeast quadrant of the mound, approximately 70 m away from the black smoker chimneys (Fig. 2). Fluids from the white smokers are zinc-rich and have lesser amounts of iron and copper than the black smoker fluids (Tivey et al., 1995).

Seventeen holes were drilled in five areas of the mound, with the deepest penetration of 125 m (Fig. 2). Areas drilled, include the high-temperature black smoker complex and a lower temperature white smoker vent field, reveal a multistage depositional history, complex fluid interactions, and the extent of subseafloor mineralization and associated alteration (Humphris, Herzig, Miller, et al., 1996; Humphris et al., 1995). Detailed lithologic and petrographic descriptions of the rock units from the TAG mound and underlying alteration zone are presented in Humphris, Herzig, Miller, et al. (1996) and Humphris et al. (1995) and will only be summarized here.

A schematic view of the geology of the TAG mound and the underlying alteration zones is given in Figure 3. The upper 10–20 m of the TAG mound consists of massive pyrite (Pl. 1, Fig. 1) and pyrite breccias with significant chalcopyrite and sphalerite in places. These are underlain by pyrite-anhydrite breccias (Pl. 1, Fig. 2) from about 20 to 30 meters below seafloor (mbsf). Pyrite-silica breccias (Pl. 1, Fig. 3) at the top of the stockwork grade into silicified wallrock breccias below 40 m (Pl. 1, Fig. 4). Chloritized basalt breccias (Pl. 1, Fig. 5) were sampled at depths greater than 100 m. Recovery of relatively unaltered basalt near the edges of the mound has constrained the extent of the stockwork mineralization and intense alteration to a pipe-like feature of about 80 m diameter.

Detailed core logging revealed 5 stages of veining in the footwall alteration zone. Differentiation of stringer veins is based on consistent crosscutting relationships, mineralogy, and vein selvage and alteration characteristics. Veining at TAG consists of anhydrite veins in the upper portions of the mound passing downwards into a quartz stockwork with late anhydrite veins in the stringer zone. The earliest veins recognized (Stage 1) are very thin veins of dark green chlorite occurring within fragments of green chloritized basalt. Stage 2 is characterized by 0.5- to 3-cm zones gray quartz with abundant disseminated pyrite and local chalcopyrite veins (Pl. 1, Fig. 4). Stage 3 consists of less than 2- to 3-mm-wide, pyrite-filled fractures. White quartz and pyrite, up to 2 cm wide, are the primary constituents of the Stage 4 veins (Pl. 1, Fig. 5). Stage 5 consists of anhydrite veins up to 45 cm thick, many of which have a chalcopyrite selvage and a pyritization halo (Pl. 1, Fig. 6).

SULFUR-ISOTOPE GEOCHEMISTRY

The drilling at TAG offers the first opportunity for a detailed study (laterally and vertically) of sulfur-isotope variation of the various mineralization textures, stockwork veins, and alteration sulfides within a modern seafloor hydrothermal mound and its underlying stockwork zone. In this study four textural types of sulfides were analyzed. These are (1) massive sulfide, (2) sulfide clasts from the various breccias types, (3) disseminated sulfides associated with alteration, and (4) veins, including vein selvages and halos. Pyrite, chalcopyrite, and rare sphalerite were analyzed. Anhydrites from the pyrite-anhydrite breccias and Stage 5 anhydrite veins were also analyzed. Table 1 lists the geologic characteristics of the samples analyzed and examples of the various textural types of sulfides and sulfates analyzed in this study are shown in Pl. 1.

Methods

For each sample the sulfide or sulfate was hand picked or drilled out with the aid of a small-diameter dentist drill. Petrographic examination aided selection of sample sites that were monomineralic. The drill was cleaned between each sample extraction to ensure no cross-sample contamination. Hand-picked or drilled mineral separates were combusted with excess CuO in vacuo to produce SO_2 by the method of Fritz et al. (1974). Sulfur-isotope analyses were performed in the Central Science Laboratory at the University of Tasmania on a VG ISOGAS stable isotope mass spectrometer. Stable isotope results are expressed in standard (δ) notation with the Canyon Diablo Troilite (CDT) used as a reference. Sample reproducibility is typically ± 0.05‰ (per mil) and analytical uncertainty is less than ± 0.02‰.

Results

Sulfur-isotope data for sulfides and sulfates from the lateral and vertical extent of the TAG mound and underlying stockwork system are given in Table 1 and Figure 4. In total, 103 sulfide (98 pyrite, 4 chalcopyrite, 1 sphalerite) and 5 sulfate samples were analyzed in this study. The overall range of sulfide $\delta^{34}S$ analyses was from 0.35‰ to 10.27‰, with a mean of 7.20‰ (Tables 1, 2). The anhydrite samples have a mean $\delta^{34}S$ value of 21.10‰ from a tight range of 20.55‰ to 21.56‰. The only previously published sulfur-isotope values for TAG samples range from 4‰ to 6‰ (n = 14), with a mean of approximately 5‰ that came from the surface of the TAG mound (Lein et al., 1993).

When the different sulfide textures are assessed, it becomes apparent that significant differences exist between the textural types (Table 2; Fig. 5). The massive sulfide and breccia clasts have a simi-

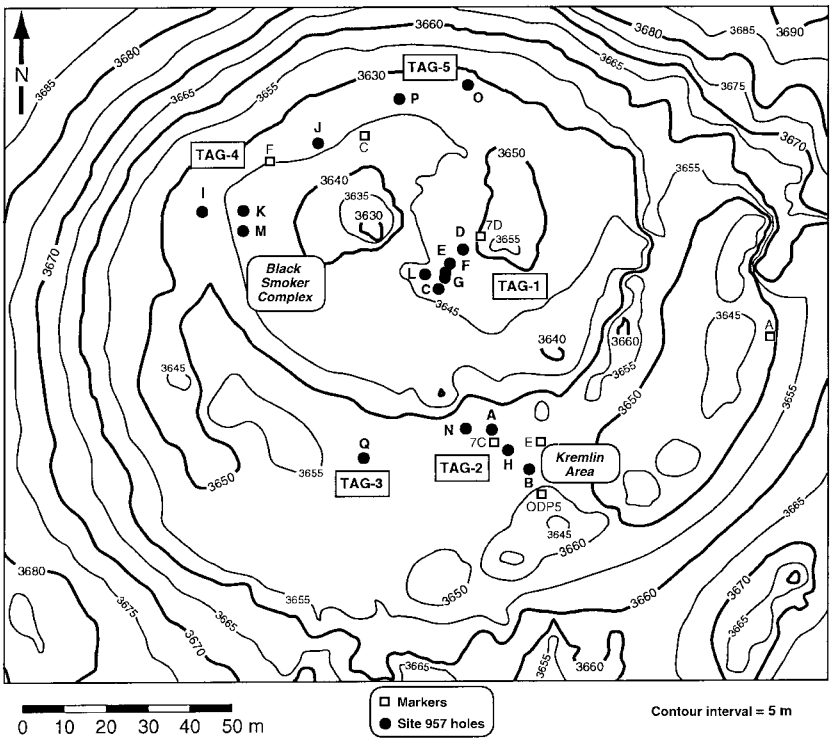

Figure 2. Bathymetric map of the TAG mound showing location of drill holes (solid circles) and areas of the mound discussed in the text. Open squares are survey markers. (From Humphris, Herzig, Miller, et al., 1996.)

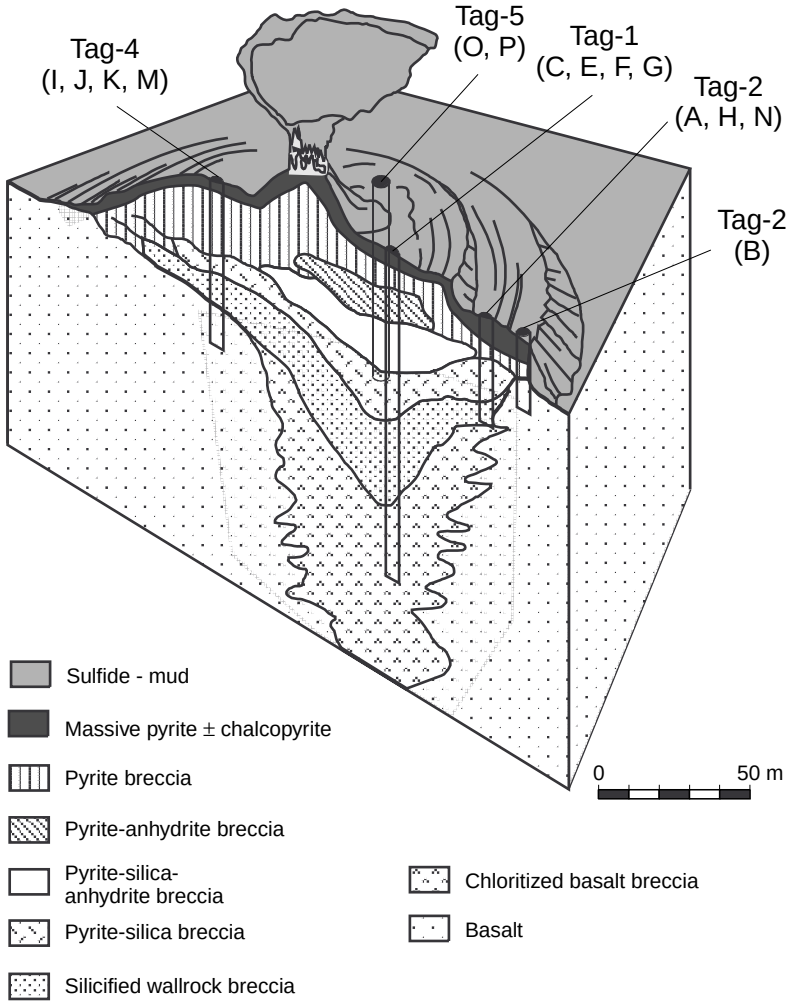

Figure 3. Schematic representation of the internal stratigraphy of the TAG mound. Locations of areas of the mound with associated drill holes (capital letters) discussed in the text are illustrated. (Modified from Humphris et al., 1995.)

Table 1. Sulfur-isotope data.

Hole, core, section	Piece	Depth (mbsf)	Mineralization type	Sulfide texture	Sulfur isotopes (‰)			
					Pyrite	Sphalerite	Chalcopyrite	Anhydrite
158-957A-								
A-1X-1	2	0.04	Porous massive pyrite	Massive	6.62			
A-3X-1	4	10.19	Porous massive pyrite	Massive	0.35			
A-3X-1	11	10.50	Porous massive sphalerite	Massive		5.82		
158-957B-								
B-1R-2	2	1.13	Porous massive pyrite	Massive	7.68			
158-957C-								
C-4W-1	2	10.52	Porous nodular pyrite breccia	Clast	7.32			
C-5N-1	4	15.21	Massive pyrite-anhydrite breccia	Clast	6.72			
C-7N-1	6E	19.94	Siliceous pyrite-anhydrite breccia	Clast	6.62			
C-7N-1	8E	20.68	Siliceous pyrite-anhydrite breccia	Clast	6.88			
C-7N-2	1F	21.59	Siliceous pyrite-anhydrite breccia	Clast	6.61			
C-7N-2	1I	21.81	Anhydrite vein	Vein Py	7.51			
C-7N-2	1K	22.12	Siliceous pyrite-anhydrite breccia	Clast, vein	5.74			20.78
C-7N-3	4A	22.61	Siliceous pyrite-anhydrite breccia	Clast, vein	6.44			21.38
C-8W-1	1	19.50	Siliceous pyrite-anhydrite breccia	Clast	6.78			
C-10N-1	3	28.81	Massive pyrite breccia	Massive	7.25			
C-11N-1	3F	31.39	Pyrite-silica-anhydrite breccia	Clast	6.93			
C-11N-1	3I	31.65	Anhydrite vein	Vein Py	5.51			
C-11N-2	1B,C	32.19	Pyrite-silica-anhydrite breccia	Clast, vein halo, vein	6.01		7.41	21.56
C-11N-2	10	33.44	Pyrite-silica-anhydrite breccia	Clast	5.80			
C-11N-3	2A,B,C	33.63	Anhydrite vein	Py halo	6.92			
C-11N-3	10A	34.64	Pyrite-silica breccia	Clast, vein selvage	8.30		6.09	
C-12N-2	6	36.05	Pyrite-silica-anhydrite breccia, veined	Clast	6.51			
C-12N-3	2	36.58	Pyrite-silica-anhydrite breccia	Clast, Cp in vein	6.11		5.64	
C-13N-1	17A,B	38.19	Pyrite-silica breccia	Clast	6.22			
C-13N-2	3A	38.71	Anhydrite vein	Py halo, Cp selvage, vein	6.10		6.23	21.25
C-13N-2	3C	38.81	Pyrite-silica breccia	Clast	7.30			
C-14N-2	1C	41.12	Anhydrite vein	Py + Cp in vein	6.36#			
C-15N-1	11A-F	42.94	Silicified wallrock breccia	Clast	6.61			
C-15N-4	4	46.10	Pyrite-silica breccia	Clast	7.15			
C-16N-1	5A-D	46.48	Pyrite-silica breccia	Clast	7.32			
C-16N-1	16	47.47	Silicified wallrock breccia	Clast	7.63			
C-16N-2	7A,B	48.29	Silicified wallrock breccia	Dissem in matrix	8.27			
158-957E-								
E-1R-1	4	31.70	Pyrite-silica breccia	Clast	7.89			
E-5R-1	6	58.87	Pyrite-silica breccia	Clast	7.60			
E-7R-1	1	68.30	Pyrite silica breccia	Vein Py, clast	6.53, 7.76			
E-9R-1	1	77.80	Massive granular pyrite	Massive	6.45			
E-11R-1	6	87.34	Silicified wallrock breccia	Dissem in matrix	7.15			
E-12R-1	2	91.89	Silicified wallrock breccia, anhydrite vein	Vein selvage, vein	7.10			20.55
E-14R-1	9	101.86	Chloritized basalt breccia	Dissem in alteration	7.74			
E-17R-1	4	116.25	Chloritized basalt breccia	Dissem in alteration	8.85			
E-17R-1	7	116.37	Chloritized basalt breccia	Vein Py	8.41			
E-18R-1	9	121.13	Chloritized basalt breccia	Clot in alteration	8.41			
158-957F-								
F-1N-1	6	1.23	Massive granular pyrite	Massive	6.74			
F-1N-1	10A-D	1.41	Nodular pyrite breccia	Nodule	7.14			
F-2N-1	7	5.86	Massive granular pyrite	Massive	7.17			
158-957G-								
G-1N-1	3	12.10	Massive granular pyrite	Massive	6.49			
G-3N-1	4A-D	21.35	Nodular siliceous pyrite-anhydrite breccia	Clast	8.30			
158-957H								
H-1N-1	5	8.84	Porous massive pyrite	Massive	7.78			
H-1N-1	12	9.23	Porous nodular pyrite breccia	Clast	7.59			
H-2N-1	1	13.20	Porous nodular pyrite breccia	Clast	7.73			
H-3N-1	4	17.87	Porous nodular pyrite breccia	Clast	7.91			
H-5N-1	5A,B,C	26.98	Pyrite-silica breccia	Clast	7.64			
H-5N-2	1D	27.85	Silicified wallrock breccia	Dissem in alteration	7.79			
H-5N-2	3A,B,C	28.17	Silicified wallrock breccia	Vein Py	6.05			
H-6N-1	1	31.20	Pyrite-silica breccia	Nodule	8.29			
H-8N-1	3	40.34	Pyrite-silica breccia	Dissem in alteration	8.04			
H-8N-1	10	40.86	Massive granular pyrite	Massive	8.18			
H-8N-1	14	41.10	Pyrite-silica breccia	Dissem in alteration	8.49			
158-957I-								
I-1N-1	1	9.00	Porous massive pyrite	Massive	7.60			
I-1N-1	8	9.47	Porous massive pyrite	Massive	6.91			
I-1N-1	12	9.75	Pyrite-silica breccia	Dissem in alteration	8.47			
158-957K-								
K-1X-1	3	0.14	Porous massive pyrite	Massive	7.45			
K-2N-1	3	10.08	Massive granular pyrite	Massive	7.58#			
K-2N-1	11	10.46	Massive granular pyrite	Massive	8.16			
K-3X-1	4	14.66	Massive pyrite	Massive	7.44			
158-957M								
M-1R-2	6	0.79	Pyrite-silica breccia	Dissem in alteration	8.08			
M-2R-1	1	9.30	Porous massive pyrite	Massive	7.58			
M-2R-1	8	9.65	Pyrite-silica breccia	Clast	7.24			
M-3R-1	12	14.75	Porous massive pyrite	Massive	6.81			
M-3R-1	19	15.08	Pyrite-silica breccia	Vein, dissem in alteration	6.62, 9.29			
M-3R-1	30	15.60	Pyrite-silica breccia	Vein	6.88			
M-3R-2	2		Pyrite-silica breccia	Vein	7.16			
M-4R-1	11	19.78	Pyrite-silica breccia	Dissem in alteration	8.42			

Table 1 (continued).

Hole, core, section	Piece	Depth (mbsf)	Mineralization type	Sulfide texture	Sulfur isotopes (‰)			
					Pyrite	Sphalerite	Chalcopyrite	Anhydrite
M-5R-1	13	25.03	Silicified wallrock breccia	Dissem in alteration	8.64			
M-6R-1	4	29.45	Silicified wallrock breccia	Vein	7.34			
M-7R-1	4	34.48	Silicified wallrock breccia	Dissem in alteration	8.49			
M-8R-1	4	38.47	Silicified wallrock breccia	Dissem in alteration	8.15			
M-9R-1	4	42.17	Silicified wallrock breccia	Dissem in alteration	8.20			
158-957N-								
N-1W-1	4	0.23	Pyrite-silica-anhydrite breccia	Clast	7.37			
158-957O-								
O-3R-1	2	10.95	Pyrite-anhydrite breccia	Nodule	7.14			
O-4R-1	4	16.02	Pyrite-anhydrite breccia, vein related	Clot in vein	6.43#			
O-4R-1	14	16.54	Pyrite-anhydrite breccia, vein related	Clot in vein	6.92			
O-4R-1	16	16.63	Pyrite-silica breccia	Dissem in alteration	8.10			
158-957P-								
P-1R-1	5	0.24	Pyrite-anhydrite breccia	Dissem in alteration	10.27			
P-1R-1	10	0.55	Pyrite-anhydrite breccia	Clast	6.99			
P-3R-1	2	11.95	Massive granular pyrite	Massive	6.82			
P-5R-1	2	21.57	Massive granular pyrite	Massive	5.71			
P-8R-1	1	35.10	Massive granular pyrite	Massive	6.94			
P-8R-1	4	35.23	Pyrite-silica breccia	Clast	7.02			
P-9R-1	3	40.26	Massive granular pyrite	Massive	7.32			
P-10R-1	5	45.29	Pyrite-silica breccia	Vein + dissem in alteration	7.41			
P-11R-1	9	50.51	Pyrite-silica breccia	Vein + dissem in alteration	7.11			
P-12R-2	1	55.64	Massive granular pyrite	Massive	6.84#			
P-12R-2	6	55.89	Pyrite-silica breccia	Dissem in alteration	8.32			
P-12R-3	2	56.93	Pyrite-silica breccia	Clast	7.73			
P-12R-4	1	57.39	Silicified wallrock breccia	Vein	6.97			
P-12R-4	5	57.61	Massive granular pyrite	Massive	7.08			
158-957Q-								
Q-2R-1	3	9.58	Massive porous pyrite	Vein	7.49			

Notes: * = texture of material analyzed, # = mixture of pyrite and chalcopyrite. Abbreviations: Sect. = Section, Py = pyrite, Cp = chalcopyrite, dissem = disseminations.

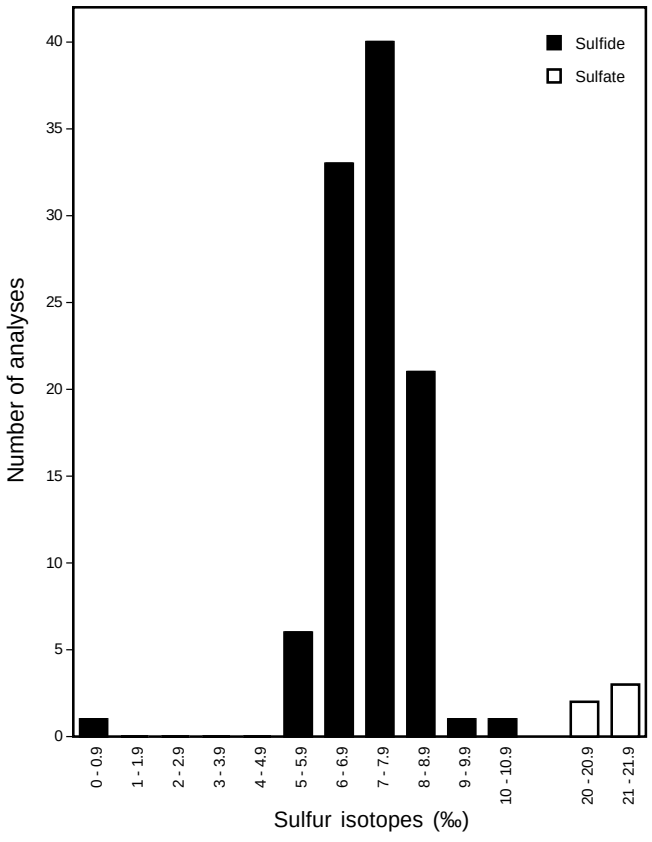

Figure 4. Histogram of the sulfur-isotope values for all sulfide and sulfate samples used in this study. Data from Table 1.

Table 2. Sulfur-isotope summary statistics.

Sample type	n	Mean (‰)	Minimum (‰)	Maximum
Sulfides				
Overall	103	7.20	0.35	10.27
Massive sulfide	24	7.07	0.35	8.18
Breccia clasts	36	7.05	5.74	8.30
Disseminations	21	8.40	7.15	10.27
Vein*	22	6.70	5.51	7.51
Sulfate				
Overall	5	21.10	20.55	21.56

Note: n = number of analyses, * = includes sulfides in vein, vein selvage, and vein halo.

lar distribution of isotope values ($\delta^{34}S$ = 6‰–8‰); however, the $\delta^{34}S$ values of the disseminated pyrite associated with the alteration are distinctly heavier ($\delta^{34}S$ = 8‰–10‰). Vein sulfides have the lightest $\delta^{34}S$ values ($\delta^{34}S$ = 5‰–7‰) at TAG.

1. Massive Sulfide

Pyrite in the massive sulfide (Pl. 1, Fig. 1) from the upper portions of the mound (Fig. 3) have $\delta^{34}S$ values that range between 0.35‰ and 8.18‰, with a mean of 7.07‰. The pyrite is fine to medium grained, granular, homogeneous, with variable porosity. Primary, colloform-banded textures are preserved only locally in the more massive samples.With the exception of one sphalerite (Sample 158-957A-3X-1, Piece 1, 50.0–58.0 cm; 10.50 mbsf) all samples analyzed were pyrite (Table 1). Twenty-four of the 25 samples analyzed fall between 5.71‰ and 8.18‰ with one (Sample 158-957A-3X-1, Piece 4, 18.5–23.5 cm; 10.19 mbsf) having the lightest $\delta^{34}S$ value (0.35‰) measured at TAG (Table 1).

2. Breccia Clasts

Pyrite breccias are the dominant lithology between 15 and 40 mbsf. These breccias include all fragments and clasts of pyrite (Pl. 1,

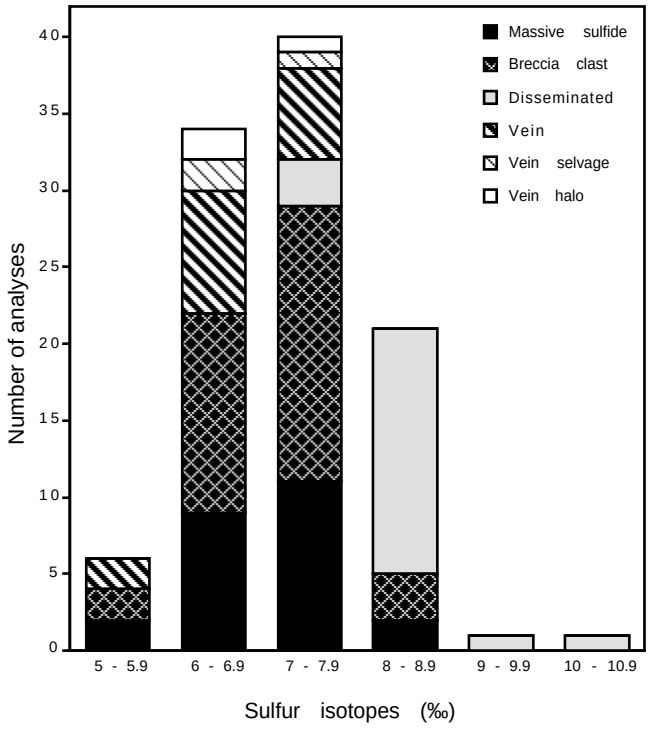

Figure 5. Distribution of sulfide (primarily pyrite) sulfur-isotope values of specific textures within the TAG mound and underlying stockwork zone. Data from Table 1.

Figs. 2, 3) within the various breccias of the mound (pyrite breccia, pyrite-anhydrite breccia, pyrite-silica breccia) and stringer zone (silicified wallrock breccia and chloritized basalt breccia; Fig. 2). The pyrite-silica-anhydrite breccias consist mainly of pyritic and siliceous clasts cemented by quartz and anhydrite matrix and veins. Pyrite-silica breccias consist mainly of quartz-pyrite clasts in a quartz matrix. All samples analyzed for $\delta^{34}S$ were pyrite. The range of $\delta^{34}S$ values for the breccia clasts varies from 5.74‰ to 8.30‰, with a mean of 7.05 ‰. These breccia clasts have a similar sulfur-isotope signature to the massive sulfide.

3. Disseminated Sulfides Associated with Alteration

The heaviest sulfur-isotope values at TAG come from fine-grained, disseminated pyrite associated with siliceous and chloritic alteration in the deeper portions of the mound and the underlying stockwork zone (Fig. 2; Pl. 1, Fig. 4). Larger fragments of wallrock are intensely fractured, veined by quartz, and contain widespread disseminated pyrite and small pyrite aggregates. Fine-grained, disseminated pyrite occurs throughout the alteration and rims the wallrock fragments. Sulfur-isotope values from the disseminated pyrite are the heaviest at TAG, averaging 8.40‰, from a range of 7.15‰ to 10.27‰.

4. Veins

Sulfides in the deep quartz-pyrite stringer veins (Stages 2–4) and the anhydrite veins (Stage 5) from within the mound have, on average, the lightest sulfur-isotope values at TAG. Pyrite and chalcopyrite (Table 1) from within the veins, vein selvages, and vein halos (Pl. 1, Figs. 5, 6) have $\delta^{34}S$ values that vary from 5.51‰ to 7.54‰, with a mean of 6.70‰. Vein sulfides (pyrite and chalcopyrite) were analyzed separately from the selvage sulfides (pyrite and chalcopyrite) and halo sulfides (pyrite), and show vein sulfides to have a $\delta^{34}S$ mean of 6.75‰ compared to the selvages (6.81‰) and the halo (6.47‰) (Table 1). Figure 6 illustrates the distribution of $\delta^{34}S$ values from a Stage 5 anhydrite vein with a well-developed chalcopyrite selvage and pyritization halo that grades into a pyrite-silica breccia. The chalcopyrite selvage has a slightly heavier sulfur-isotope signature (6.23‰) compared to the pyritization halo (6.10‰). The pyritization halo pyrite has a significantly lighter $\delta^{34}S$ value compared to the pyrite breccia clasts (7.30‰) in the pyrite-silica breccia host rock.

Spatial Distribution of $\delta^{34}S$ Values

TAG-1 Area

The TAG-1 area, located 20 m east-southeast of the Black Smoker Complex, includes Holes 957C, 957D, 957E, 957F, 957G, and 957L (Fig. 2). These holes are aligned in a northeasterly direction in an area measuring roughly 10 × 5 m. No core was recovered from Holes 957D and 957L. Hole 957E had the deepest penetration of 125 m into the TAG hydrothermal system.

The holes in the TAG-1 area form a composite section through the hydrothermal mound and into the upper portions of the stockwork zone (Fig. 3). The rock types are, with increasing depth, massive porous to granular pyrite ± chalcopyrite, pyrite breccias and pyrite sand, pyrite-anhydrite breccias, pyrite-silica breccias, silicified wallrock breccias, and chloritized basalt breccias. Anhydrite veining (Stage 5) is abundant throughout the vertical extent of the core, but is best developed in the pyrite-anhydrite and pyrite-silica breccias. A quartz stockwork (Stages 2–4) occurs within the silicified wallrock and chloritized basalt breccias.

The vertical distribution of $\delta^{34}S$ values for the four different textural types of sulfides analyzed at TAG-1 is shown in Figure 7. In general, the overall trend is for the sulfur-isotope values to become heavier with depth. Disseminated pyrite within the siliceous matrix of the silicified wallrock breccias and the chloritic alteration of the chloritized basalt breccias have the heaviest $\delta^{34}S$ values. Pyrite in breccia clasts throughout the vertical extent of the core from TAG-1 does not show any consistent variation either between the different breccia types or with depth. Vein pyrite and chalcopyrite generally have lighter $\delta^{34}S$ values compared to the massive sulfide and the breccia clasts, except for a deep vein (Sample 158-957C-17R-1, Piece 4, 39.0–44.0 cm; 116.37 mbsf) in the chloritized basalt breccia that has a relatively heavy sulfur-isotope value ($\delta^{34}S$ = 8.41‰).

TAG-2 Area

Holes 957A, 957B, and 957H in the TAG-2 area are located on the lower terrace of the mound, within approximately 10 m of each other in the Kremlin white smoker field (Fig. 2). TAG-2 is located approximately 60 m southeast of the central Black Smoker Complex and about 20 m from the eastern edge of the mound. Hole 957H had the deepest penetration at 55 mbsf. Near the surface of the mound, iron-oxide, red-gray chert, and massive pyrite and sphalerite were recovered. With increasing depth pyrite breccia, pyrite-silica breccia, and silicified wallrock breccias were encountered. Weakly altered basalt was observed at the base of Hole 957B. In general, the pyrite breccias and pyrite silica breccias in the TAG-2 area are more uniform in geological characteristics and appeared to have experienced a less complex history of brecciation, cementation, and veining compared to rocks in either TAG-1 or TAG-4 areas (Humphris, Herzig, Miller, et al., 1996).

Sulfur-isotope values generally become heavier with depth in the TAG-2 area (Fig. 8). Massive sulfide samples, both pyrite and sphalerite (Table 1), are lighter $\delta^{34}S$ values compared to the pyrite breccia clasts. The heaviest $\delta^{34}S$ values come from disseminated pyrite in the silicified wallrock breccias.

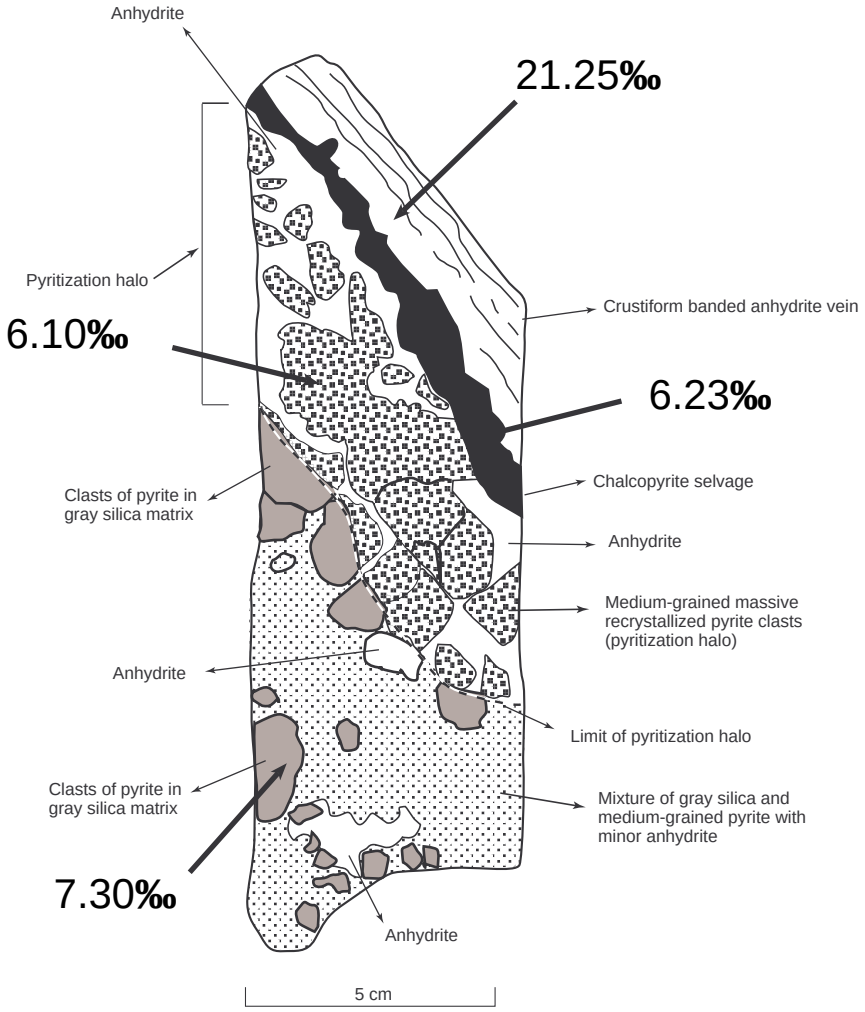

Figure 6. Distribution of $\delta^{34}S$ values in a Stage 5 anhydrite vein with a well-developed chalcopyrite selvage and pyritization halo that grades into a pyrite-silica breccia (Sample 158-957C-13N-2, Pieces 3A-3C, 15.0–33.0 cm; 38.71 mbsf). The chalcopyrite selvage has a slightly heavier sulfur-isotope signature compared to the pyritization halo. The pyritization halo pyrite has a significantly lighter sulfur-isotope value compared to the pyrite breccia clasts in the pyrite-silica breccia. (Modified from Humphris, Herzig, Miller, et al., 1996).

TAG-3 Area

The TAG-3 area is located on the lower terrace of the mound approximately 55 m south of the black smoker terrace (Fig. 2). As the only material recovered in Hole 957Q were drill cuttings and a few small fragments of red and gray chert and partially silicified iron oxides, no sulfur-isotope analyses were undertaken.

TAG-4 Area

Holes 957I, 957J, 957K, and 957M were drilled on the upper terrace on the western side of the mound in the area designated as TAG-4 (Fig. 2). Core recovered from TAG-4 indicates that the upper 10 m of the mound consists of massive sulfide (pyrite and marcasite) with red and gray chert, followed by a 10-m-thick zone of massive pyrite and pyrite breccia that grades downwards into pyrite-silica breccias. Underlying the pyrite-silica breccias are silicified wall rock breccias, which are in sharp contact with weakly altered basalt.

The vertical distribution of $\delta^{34}S$ values for the four different textural types of sulfides analyzed at TAG-4 is shown in Figure 9. Overall there is a tendency for the sulfur-isotopes to become heavier with depth, but this increase is less pronounced when compared to the TAG-1 and TAG-2 areas. Massive sulfide and breccia clasts have a similar range and distribution of $\delta^{34}S$ values, but the disseminated pyrite associated with alteration have heavier $\delta^{34}S$ values.

TAG-5 Area

The TAG-5 area is located near the margin of the upper terrace on the north side of the mound approximately 20–30 m northeast of the Black Smoker Complex. Holes 957O and 957P were drilled at TAG-5. The rock types found with increasing depth were massive pyrite, pyrite-anhydrite breccias, pyrite-silica breccias, and silicified wall-rock breccias. The overall stratigraphy at TAG-5 is similar to that at TAG-1.

Figure 10 shows the sulfur-isotope values at TAG-5. The heaviest $\delta^{34}S$ value (10.27‰) measured in this study comes from disseminated pyrite in the matrix of a pyrite-anhydrite breccia (Sample 158-957P-1R-1, Piece 5, 24.0–30.0 cm; 0.24 mbsf) near the top of the mound. There is a weak correlation of heavier $\delta^{34}S$ values with depth at TAG-5, similar to the $\delta^{34}S$ distribution in the TAG-4 area. The heaviest $\delta^{34}S$ values are from the disseminated sulfides associated with alteration and the lightest values are from vein sulfides.

Comparison with Other Modern and Ancient Seafloor Deposits

Sulfur-isotope data for sulfide and sulfate minerals precipitated at modern seafloor hydrothermal sites are illustrated in Figure 11. The $\delta^{34}S$ values for sulfides for unsedimented ridges range from approximately –1‰ to 8‰; however, the range for sedimented ridges is –4‰ to 1‰ (Böhlke and Shanks, 1994; Duckworth et al., 1995; Shanks et

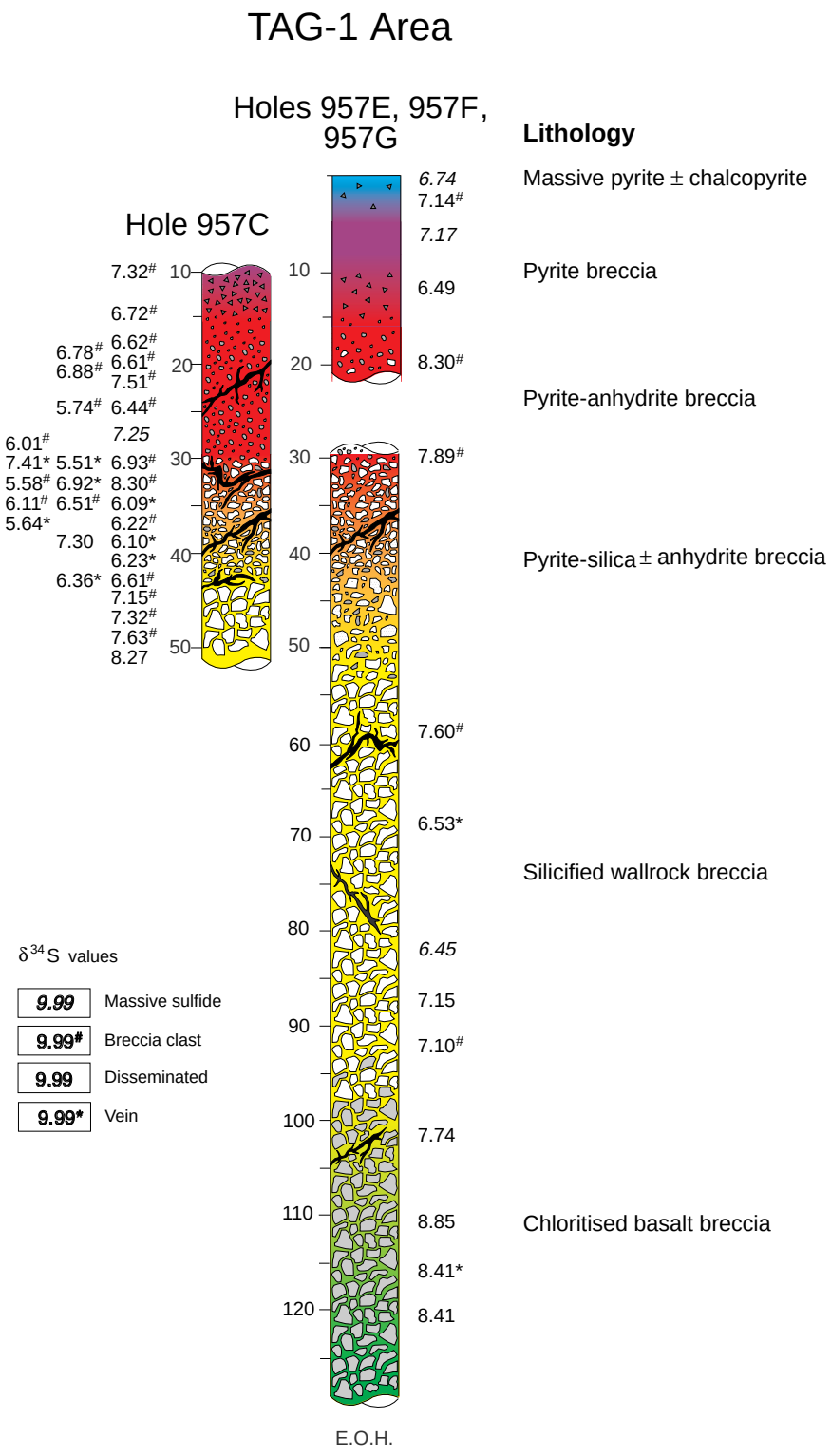

Figure 7. Distribution of $\delta^{34}S$ values, by textural type, for the TAG-1 area. Position of analyses corresponds to sample location within mound and stockwork zone. Depths given are in mbsf (see Table 1). Excellent core recovery in Hole 957C allowed abundant sampling. (Modified from Humphris, Herzig, Miller, et al., 1996). E.O.H. = end of hole.

al., 1995). In comparison, sulfides from seafloor hydrothermal systems forming in backarc environments of the Western Pacific have $\delta^{34}S$ values that range from –2‰ to +11‰ (Gemmell et al., 1996).

A comparison of the data in Figure 11 shows that the sulfur-isotope values measured at TAG are some of the heaviest recorded for unsedimented mid-ocean ridge deposits. Higher sulfide values have been reported in sedimented ridge settings, such as Escanaba Trough and Middle Valley. Care must be taken, however, when interpreting these data in Figure 11 as all the samples analyzed from the various seafloor sites (Fig. 11) have come from surface samples and the heaviest $\delta^{34}S$ values from TAG come from disseminated sulfides associated with alteration from the base of the mound and in the underlying stockwork system.

Ancient volcanic-hosted massive sulfide mineralization considered to form at or near seafloor spreading systems (ophiolites) is found in Cyprus, Oman, and Newfoundland. The sulfur-isotope values for pyrite from the massive sulfide deposits hosted in the Troodos ophiolite, Cyprus, range from 0.4‰ to 7‰ (n = 45), with a mean of

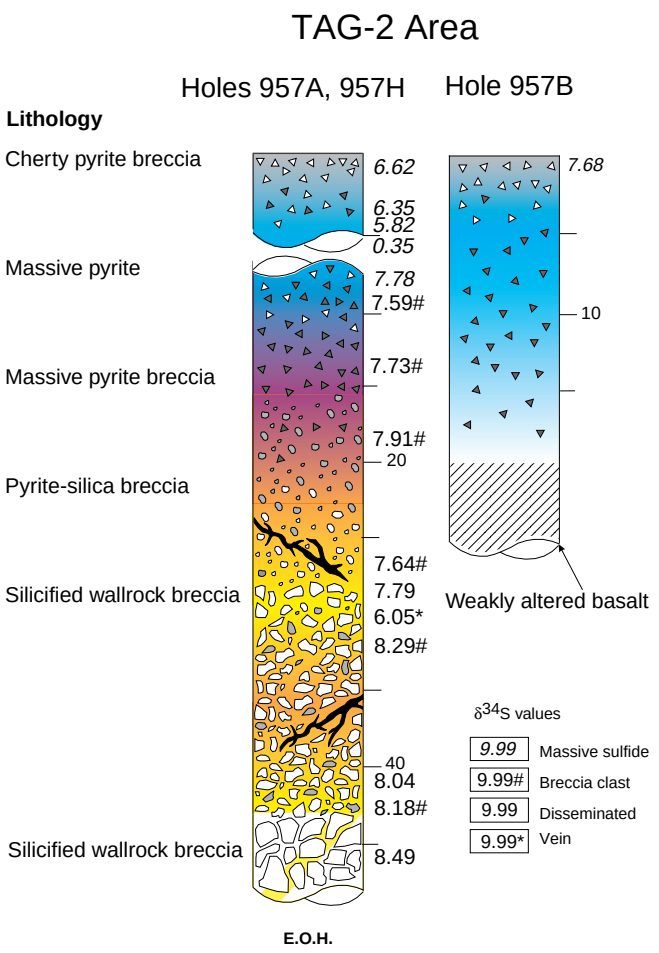

Figure 8. Distribution of $\delta^{34}S$ values, by textural type, for the TAG-2 area. Position of analyses corresponds to sample location within mound and stockwork zone. Depths given are in mbsf (see Table 1). (Modified from Humphris, Herzig, Miller, et al., 1996.)

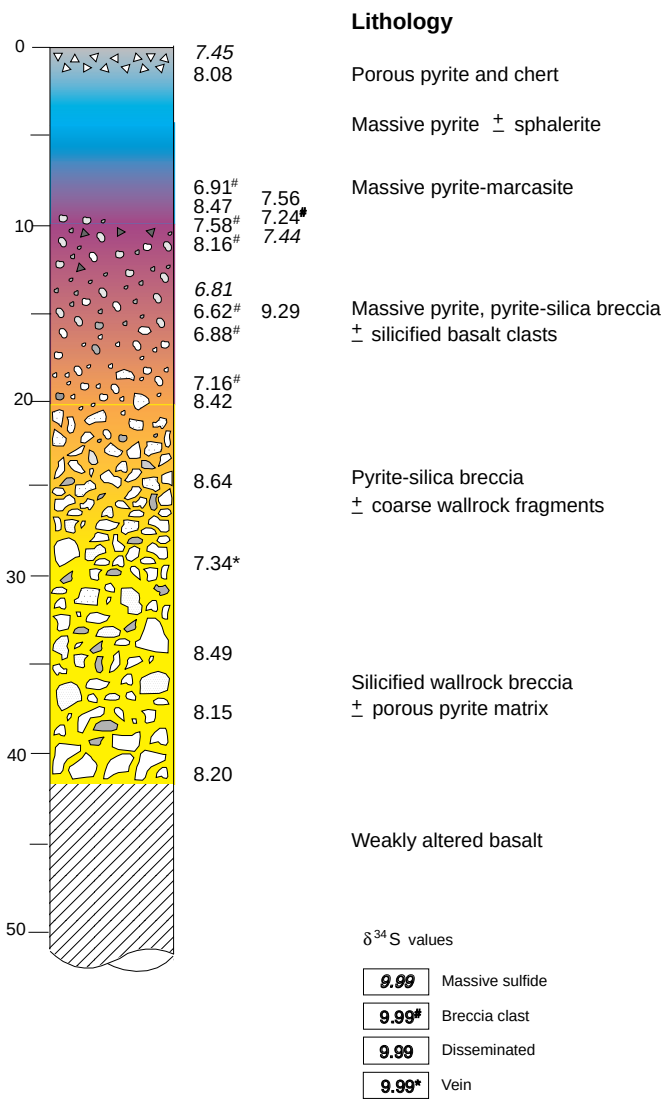

Figure 9. Distribution of $\delta^{34}S$ values, by textural type, for the TAG-4 area. Position of analyses corresponds to sample location within mound and stockwork zone. Depths given are in mbsf (see Table 1). (Modified from Humphris, Herzig, Miller, et al., 1996.)

4.2‰ (Spooner, 1977). Bettison-Varga et al. (1994) report heavier $\delta^{34}S$ values of 5.0‰ to 9.0‰ (n = 8), averaging 7.2‰ for pyrites in the massive sulfide mineralization of the Troodos ophiolite. Franklin et al. (1981) reports that there is no significant difference in sulfur-isotope values between the massive, fracture-filling, cavity-filling, and disseminated ores at Troodos, but that there is a slight difference in average sulfur composition between individual deposits.

Volcanic-hosted Fe-Cu-Zn massive sulfide deposits in the Oman ophiolite have $\delta^{34}S$ values varying between 1.9‰ and 8.0‰ (Haymon et al., 1989). Ophiolite-hosted cuperiferous pyrite deposits from the Notre Dame Bay, Newfoundland, have a wide range of $\delta^{34}S$ values between 5.5‰ to 23.0‰ (Bachinski, 1977).

SULFUR-ISOTOPE MODEL

Ohmoto (1986) and Taylor (1987) summarized the suggested origins of sulfur in volcanic-hosted massive sulfide deposits. These include bacterial reduction of seawater sulfate, magmatic-hydrothermal fluids, inorganic reduction of seawater sulfate (± leached magmatic sulfide), and leaching of sulfate minerals, followed by partial reduction. It is generally considered that the two main sources of sulfur in unsedimented ridge, seafloor massive sulfide systems are the reduction of seawater sulfate and magmatic sulfur, derived either as direct magmatic emanations, or sulfur leached from mid-ocean ridge basalts (MORB) (Ohmoto and Rye, 1979; Shanks et al., 1981; Solomon et al., 1988; Shanks et al., 1995).

Seawater in the modern ocean forms a uniform sulfur reservoir (Shanks et al., 1995). Sulfate in the modern ocean has a consistent value of 21.0‰ ± 0.2‰ (Rees et al., 1978). Sangster (1968) highlighted the importance of seawater in the formation of volcanic-hosted massive sulfide deposits with the correlation, through geologic time, between $\delta^{34}S$ values of the deposits and coeval seawater sulfate. For MORB, the average $\delta^{34}S$ value for total sulfur (sulfide and sulfate) is 0.3‰ ± 0.5‰ with the sulfide fraction having an average $\delta^{34}S$ value of −0.7‰ ± 0.8‰ (Sakai et al., 1984; Shanks et al., 1995).

Vent fluids for seafloor sulfide-sulfate mineralization typically have $\delta^{34}S$ values of H_2S that range from 1.5‰ to 7‰, which are generally similar to the values for sulfides precipitated within chimneys (de Ronde, 1995). Shanks et al. (1995) consider that these $\delta^{34}S_{H2S}$ values indicate that basaltic sulfur is the principal sulfur source, with

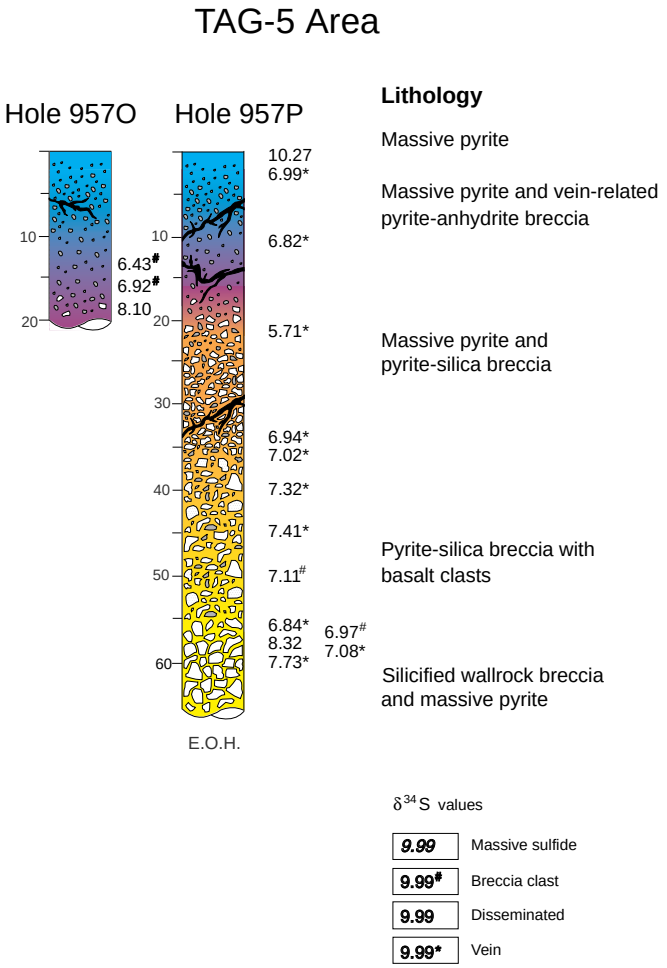

Figure 10. Distribution of $\delta^{34}S$ values, by textural type, for the TAG-5 area. Position of analyses corresponds to sample location within mound and stockwork zone. Depths given are in mbsf (see Table 1). (Modified from Humphris, Herzig and Miller, et al., 1996.)

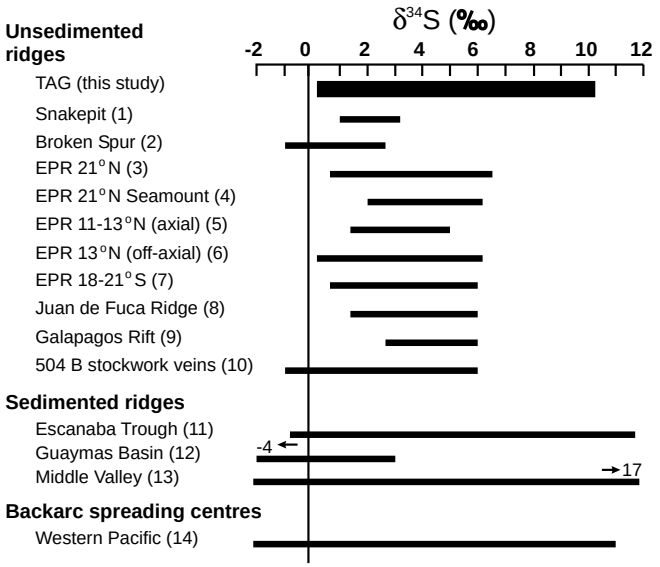

Figure 11. Comparison of TAG $\delta^{34}S$ values with sulfides from other seafloor deposits on unsedimented ridges. TAG has a similar to significantly heavier isotopic signature compared to these deposits. The $\delta^{34}S$ values for modern deposits occurring in sedimented ridge and backarc environments are given for comparison. EPR = East Pacific Rise. Data from: (1) Duckworth et al. (1995); (2) Kase et al. (1990); (3) Woodruff and Shanks (1988); (4) Alt (1988); (5) Bluth and Ohmoto (1988); (6) Knott (pers. comm. in Duckworth et al. (1995); (7) Marchig et al. (1990); (8) Shanks and Seyfried (1987); (9) Knott et al. (1995); (10) Alt et al. (1989); (11) Böhlke and Shanks (1994); (12) Shanks et al. (1995); (13) Goodfellow and Blaise (1988) and Duckworth et al. (1994); (14) Gemmell et al. (1996).

a small but detectable component from seawater sulfate inorganically reduced to H_2S. No $\delta^{34}S$ values of H_2S for the TAG vent fluids are available from the literature.

The two initial sources of sulfur during the life of the TAG hydrothermal system are seawater ($\delta^{34}S$ = 21‰) sulfate and MORB-derived sulfur ($\delta^{34}S$ = 0‰–1‰). Shanks et al. (1995) summarized the processes affecting the sulfur budget that occur during circulation of seawater in mid-ocean ridge hydrothermal systems. These processes are separated into the recharge zone, high-temperature reaction zone, and discharge zone. In the recharge zone the heating of seawater ($\delta^{34}S$ = 21‰), causes anhydrite precipitation and water/rock reactions (precipitation of magnesium-hydroxysulfate), which are effective mechanisms for limiting the amount of seawater sulfate entering the high-temperature reaction zone (Shanks et al., 1995). In the reaction zone seawater sulfate reduction occurs through the oxidation of Fe^{2+} (magnetite and olivine) in MORB (Shanks et al., 1981). During water/rock interactions in a MORB environment, seawater reacts with magmatic monosulfide solution (MSS) and/or pyrite and causes the release of H_2S to the hydrothermal fluid that has a $\delta^{34}S$ value of 1‰–1.5‰ (Woodruff and Shanks, 1988; Alt, 1995; Shanks et al., 1995). In the discharge zone (chimney environment), the hydrothermal fluid mixes with seawater causing minor sulfate reduction with $\delta^{34}S$ values of vent fluids increasing up to a maximum of approximately 4.5‰ (Janecky and Shanks, 1988). However, where vent fluids have $\delta^{34}S$ values greater than 4.5‰, Janecky and Shanks (1988) concluded that near-surface fluid/rock interactions between seawater and basaltic silicates and oxides in the feeder zone have caused the increase in $\delta^{34}S$ of vent fluids.

At TAG, any sulfur-isotope model must account for the heavy $\delta^{34}S$ signature (compared to other sediment-free hydrothermal systems, Fig. 11), the distribution of $\delta^{34}S$ values of the various textural styles (Fig. 5), and the spatial distribution of the $\delta^{34}S$ values both laterally and vertically throughout the mound and underlying stockwork zone (Fig. 12). If the deep subseafloor processes affecting the sulfur-isotope signature of the upwelling hydrothermal fluids as outlined by Alt (1995) and Shanks et al. (1995) are correct, then the initial hydrothermal fluids entering the TAG system at depth had a $\delta^{34}S$ value of approximately 0‰–1‰. This fluid mixes with locally entrained, partially reduced seawater in the upper parts of the subseafloor stockwork system (created by local hydrothermal convection though the porous and permeable mound and stockwork zone) and creates a modified hydrothermal fluid with a $\delta^{34}S$ value that is heavier ($\delta^{34}S \approx$ 6‰–7‰) than the initial hydrothermal fluid. Pyrite in the quartz-pyrite veins in the upper parts of the stockwork zone have the same $\delta^{34}S$ values ($\delta^{34}S$ = 6‰–7‰) as the modified hydrothermal fluid. The modified fluid rises to the seafloor and mixes with cold seawater which causes rapid precipitation of the massive pyrite ± chalcopyrite ($\delta^{34}S$ = 6‰–8‰) found at the top of the mound. Any anhydrite formed from the heating of entrained seawater in the massive sulfide or upper parts of the stockwork zone would have $\delta^{34}S$ values of approximately 21‰.

As TAG has had a long and complex history of waxing and waning hydrothermal activity over tens of thousands of years, there have been periods with little or no high-temperature hydrothermal upflow (Rona et al., 1993). These periods are associated with a thermal collapse accompanied by infiltration of cold seawater through the TAG

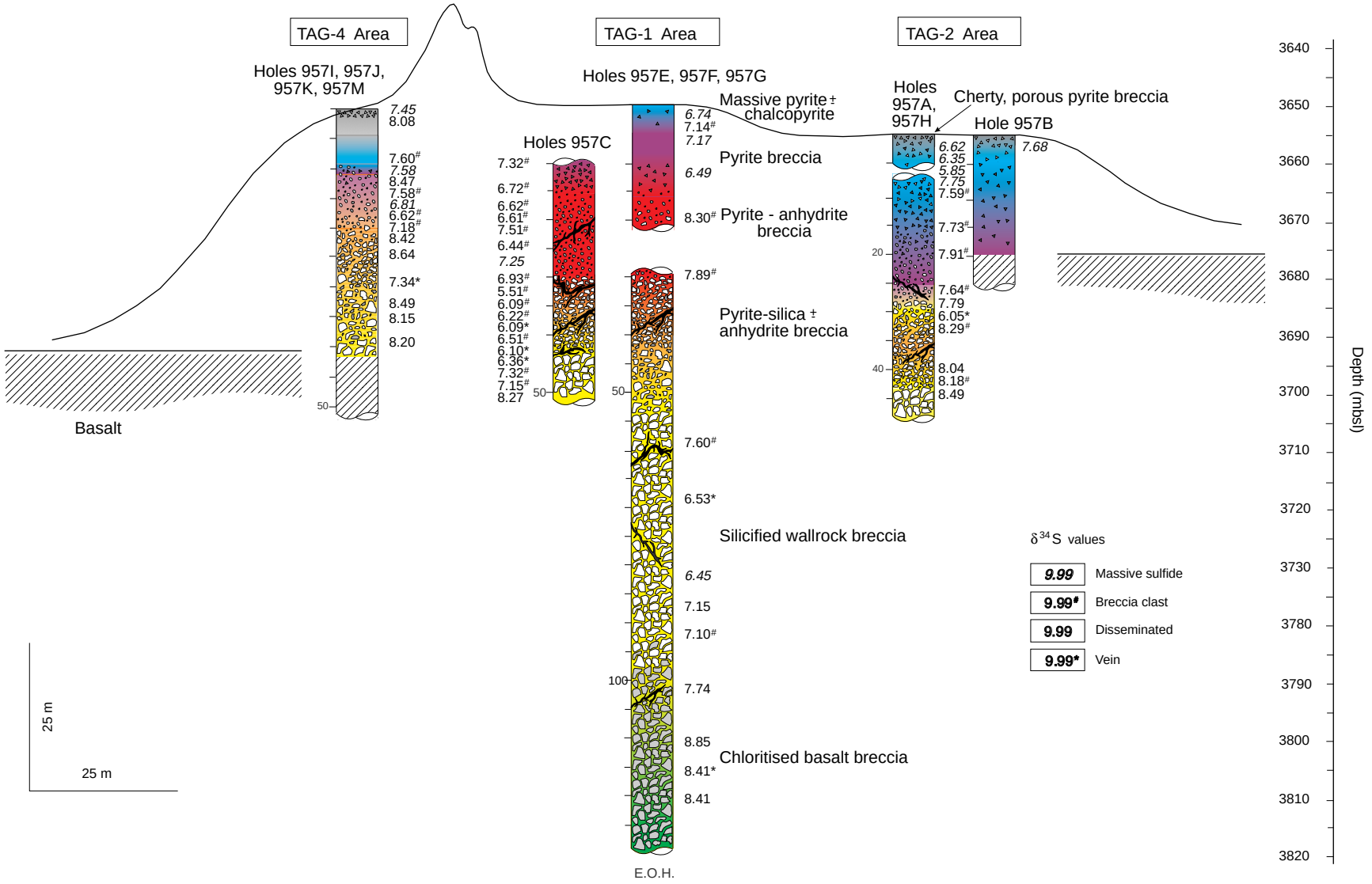

Figure 12. Distribution of $\delta^{34}S$ values, by textural type, for an east-west cross section (see Fig. 2) through the TAG mound and underlying stockwork zone. Position of analyses corresponds to sample locations, depths given are in mbsf (see Table 1). (Modified from Humphris, Herzig, Miller, et al., 1996).

mound and upper parts of the stockwork. The cold seawater dissolves anhydrite (because of the reverse solubility of anhydrite) that was within the mound and in the overlying chimneys. The dissolution of anhydrite creates clasts and fragments of pyrite ± chalcopyrite ± sphalerite on top of and within the mound.

When the hydrothermal system resumes high-temperature upflow, similar processes as those described above in the initial high-temperature phase begin operating again. Presently the hydrothermal fluid, with temperatures of between 350° and 400 °C (S. Petersen and M. Tivey, pers. comm. 1996), mixes with locally entrained partially reduced seawater in the upper parts of the subseafloor stockwork system and creates a modified hydrothermal fluid with $\delta^{34}S$ values of 6‰–7‰. This fluid passes up though the subseafloor stockwork zone and mound via veins and mixes with seawater at or near the seawater interface, causing precipitation of the massive pyrite ± chalcopyrite ($\delta^{34}S$ = 6‰–8‰) present at the top of the mound. As TAG is located on a sediment-free ridge system, there should be no biogenic processes affecting the sulfur-isotope systematics. However, the very light sulfur-isotope value for pyrite ($\delta^{34}S$ = 0.35‰) in the massive sulfide at TAG 2 (Table 1) may indicate local biogenic processes operated near the top of the mound (Shanks et al., 1995).

The rising hydrothermal fluids precipitate pyrite and quartz in the stockwork zone (vein Stages 2–4) and anhydrite ± pyrite ± chalcopyrite veins (Stage 5) within the mound. Sulfur-isotope values for sulfides ($\delta^{34}S$ = 5‰–7‰) in these veins reflect the original signature of the modified hydrothermal fluid. Anhydrite in these veins, primarily Stage 5, has $\delta^{34}S$ values of 21‰, which reflect rapid heating of entrained seawater that is infiltrating the mound. The hydrothermal fluid that is flowing through the veins leaks out though the porous and permeable mound and reacts with previously formed sulfides and sulfates creating a fluid that becomes slightly enriched in $\delta^{34}S$. This fluid is responsible for the precipitation of the disseminated pyrite associated with alteration and breccia matrix in the stockwork zone and lower portions of the mound (Fig. 3). This pyrite has the heaviest sulfur-isotope values in the TAG system ($\delta^{34}S \approx$ 8‰–10‰).

While this model has been proposed from the TAG sulfur-isotope systematics, other massive sulfide deposits where the source of the sulfur is considered to be a combination of an igneous source and seawater sulfate are, for example, Hellyer deposit, Tasmania (Gemmell and Large, 1992, 1993), South Bay deposit, Ontario (Seccombe and Clark, 1981), Big Mike deposit, Nevada (Rye et al., 1984), Buttle Lake deposits, British Columbia (Seccombe et al., 1990), and certain modern seafloor sulfide-sulfate chimneys (Styrt et al., 1981; Bluth and Ohmoto, 1988; Janecky and Shanks, 1988).

CONCLUSIONS

A detailed sulfur-isotope investigation of sulfide and sulfates within the TAG hydrothermal mound and the underlying stockwork zone has revealed that the overall range of sulfide $\delta^{34}S$ analyses is from 0.35‰ to 10.27‰, with a mean of 7.20‰. Anhydrite has a mean $\delta^{34}S$ value of 21.10‰ from a tight range of 20.55‰ to 21.56‰.

There are distinct differences in $\delta^{34}S$ values between the different textural types of pyrite (massive sulfide, breccia clasts, disseminations associated with alteration, and veins) within the hydrothermal mound and stockwork zone. The massive sulfide and breccia clasts have a similar distribution of isotope values ($\delta^{34}S$ = 6‰–8‰), however the $\delta^{34}S$ values of the disseminated pyrite associated with the alteration are distinctly heavier ($\delta^{34}S$ = 8‰–10‰). Vein sulfides have the lightest $\delta^{34}S$ values ($\delta^{34}S$ = 5‰–7‰) at TAG. A comparison of the data from the literature show that the sulfur-isotope values measured at TAG are generally the heaviest recorded for unsedimented mid-ocean ridge deposits.

A sulfur-isotope model is proposed to account for the heavy $\delta^{34}S$ signature (compared to other sediment-free hydrothermal systems), the distribution of $\delta^{34}S$ values from the various textural styles and the spatial distribution of the $\delta^{34}S$ values both laterally and vertically throughout the hydrothermal mound and underlying stockwork zone. The two initial sources of sulfur during the life of the TAG hydrothermal system are seawater sulfate ($\delta^{34}S$ = 21‰) and MORB-derived sulfur ($\delta^{34}S$ = 0‰–1‰). Variations in $\delta^{34}S$ within mound and upper parts of the stockwork zone at TAG can be explained in a model where totally to partially reduced seawater sulfate of shallow origin mixes with a deep hydrothermal fluid dominated by MORB sulfur and with previously formed sulfide and sulfate minerals in the upper parts of the stockwork zone and within the mound.

ACKNOWLEDGMENTS

JBG thanks CODES and the ODP Australian Secretariat for financial support to participate on Leg 158 and carry out this research. JBG and RS appreciate the ARC grant obtained by Professor Ross Large for development of the Central Science Laboratory stable isotope facilities at the University of Tasmania. Discussions with the Leg 158 Shipboard Scientific Party and CODES colleagues (Ross Large, Garry Davidson, Paul Kitto, Peter McGoldrick) have contributed to the ideas presented here. Sulfur-isotope analyses were completed with the help of Mike Power, Sr., and Christine Cook of the Central Science Laboratory, University of Tasmania. Debbie Harding and Stuart Smith drafted some of the diagrams. Stewart Eldridge, Laura Stokking, and the ODP editorial staff are thanked for their reviews of this paper.

REFERENCES

Alt, J.C., 1988. The chemistry and sulfur isotope composition of massive sulfide and associated deposits on Green Seamount, Eastern Pacific. *Econ. Geol.*, 83:1026–1033.

————, 1995. Subseafloor processes in mid-ocean ridge hydrothermal systems. *In* Humphris, S.E., Zierenberg, R., Mullineaux, L., and Thomson, R. (Eds.), *Seafloor Hydrothermal Systems: Physical, Chemical, Biological and Geological Interactions within Hydrothermal Systems.* Geophys. Monogr., Am. Geophys. Union, 91:85–114.

Alt, J.C., Anderson, T.F., and Bonnell, L., 1989. The geochemistry of sulfur in a 1.3 km section of hydrothermally altered oceanic crust, DSDP Hole 504B. *Geochim. Cosmochim. Acta,* 53:1011–1023.

Bachinski, D.J., 1977. Sulfur isotopic composition of ophiolitic cuperiferous iron sulfide deposits, Notre Dame Bay, Newfoundland. *Econ. Geol.,* 72: 243–257.

Bettison-Varga, L., Potts, E., Hannah, J.L. and Varga, R.J., 1994. Sulfur-isotope signatures of epidosites and massive sulfide deposits of the Troodos ophiolite, Cyprus. *Geol. Soc Am. Ann. Meet., Abstr.,* 335.

Bluth, G.J., and Ohmoto, H., 1988. Sulfide-sulfate chimneys on the East Pacific Rise, 11° and 13°N latitude. Part II: sulfur isotopes. *Can. Mineral.,* 26:505–515.

Böhlke, J.K., and Shanks, W.C., III., 1994. Stable isotope study of hydrothermal vents at Escanaba Trough: observed and calculated effects of sediment-seawater interaction. *In* Morton, J.L., Zierenberg, R.A., and Reiss, C.A. (Eds.), *Geologic, Hydrothermal and Biologic Studies at Escanaba Trough, Gorda Ridge, Offshore Northern California.* U.S. Geol. Surv. Bull., 2022:223–239.

de Ronde, C.E.J., 1995. Fluid chemistry and isotope characteristics of seafloor hydrothermal systems and associated VMS deposits: potential for magmatic contributions. *Mineral. Assoc. Can. Short Course,* 23:479–509.

Duckworth, R.C., Fallick, A.E., and Rickard, D., 1994. Mineralogy and sulfur isotopic composition of the Middle Valley massive sulfide deposit, northern Juan de Fuca Ridge. *In* Mottl, M.J., Davis, E.E., Fisher, A.T., and Slack, J.F. (Eds.), *Proc. ODP, Sci. Results,* 139: College Station, TX (Ocean Drilling Program), 373–385.

Duckworth, R.C., Knott, R., Fallick, A.E., Rickard, D., Murton, B.J., and Van Dover, C., 1995. Mineralogy and sulfur isotope geochemistry of the Broken Spur sulfides, 29°N, Mid-Atlantic Ridge. *In* Parson, L.M., Walker, C.L., and Dixon, D.R. (Eds.), *Hydrothermal Vents and Processes*. Geol. Soc. Spec. Publ. London, 87:175–189.

Franklin, J.M., Lyndon, J.W., and Sangster, D.F., 1981. Volcanic-associated massive sulfide deposits. *Econ. Geol., 75th Anniv. Vol.,* 75:485–627.

Fritz, P., Drimmie, R.J., and Nowocki, V.K., 1974. Preparation of sulfur dioxide for mass spectrometer analyses by combustion of sulfides with copper oxide. *Anal. Chem.,* 76:164.

Gemmell, J.B., Binns, R.A., and Parr, J.M., 1996. Comparison of sulfur isotope values between modern back-arc and mid-ocean ridge seafloor hydrothermal systems. *Eos,* 77:117.

Gemmell, J.B., and Large, R.R., 1992. Stringer system and alteration zones underlying the Hellyer volcanogenic massive sulfide deposit, Tasmania, Australia. *Econ. Geol.,* 87:620–649.

————, 1993. Evolution of a VHMS hydrothermal system, Hellyer deposit, Tasmania, Australia: sulfur-isotope evidence. *Res. Geol.,* 17:108–119.

Goodfellow, W.D., and Blaise, B., 1988. Sulfide formation and hydrothermal alteration of hemipelagic sediment in Middle Valley, northern Juan de Fuca Ridge. *Can. Mineral.,* 26:675–696.

Hannington, M.D., 1993. The formation of atacamite during weathering of sulfides on the modern seafloor. *Can. Mineral.,* 31:945–956.

Hannington, M.D., Thompson, G., Rona, P.A., and Scott, S.D., 1988. Gold and native copper in supergene sulfides from the Mid-Atlantic Ridge. *Nature,* 333:64–66.

Hannington, M.D., Tivey, M.K., Larocque, A.C.L., Petersen, S., and Rona, P.A., 1995. The occurrence of gold in sulfide deposits of the TAG hydrothermal field, Mid-Atlantic Ridge. *Can. Mineral.,* 33:1285–1310.

Haymon, R.M., Koski, R.A., and Abrams, M.J., 1989. Hydrothermal discharge zones beneath massive sulfide deposits mapped in the Oman ophiolite. *Geology,* 17:531–535.

Humphris, S.E., Herzig, P.M., Miller, D.J., et al., 1996. *Proc. ODP, Init. Repts.,* 158: College Station, TX (Ocean Drilling Program).

Humphris, S.E., Herzig, P.M., Miller, D.J., Alt, J.C., Becker, K., Brown, D., Brügmann, G., Chiba, H., Fouquet, Y., Gemmell, J.B., Guerin, G., Hannington, M.D., Holm, N.G., Honnorez, J.J., Itturino, G.J., Knott, R., Ludwig, R., Nakamura, K., Petersen, S., Reysenbach, A.-L., Rona, P.A., Smith, S., Sturz, A.A., Tivey, M.K., and Zhao, X., 1995. The internal structure of an active sea-floor massive sulphide deposit. *Nature,* 377:713–716.

Janecky, D.R., and Shanks, W.C., III, 1988. Computational modeling of chemical and sulfur isotopic reaction processes in seafloor hydrothermal systems: chimneys, massive sulfides, and subjacent alteration zones. *Can. Mineral.,* 26:805–825.

Kase, K., Yamamoto, M., and Shibata, T., 1990. Copper-rich sulfide deposit near 23°N, Mid-Atlantic Ridge: chemical composition, mineral chemistry, and sulfur isotopes. *In* Detrick, R., Honnorez, J., Bryan, W.B., Juteau, T., et al., *Proc. ODP, Sci. Results,* 106/109: College Station, TX (Ocean Drilling Program), 163–177.

Knott, R., Fallick, A.E., Rickard, D., and Bäcker, H., 1995. Mineralogy and sulphur isotope characteristics of a massive sulphide boulder, Galapagos Rift, 85°55′W. *In* Parson, L.M., Walker, C.L., and Dixon, D.R. (Eds.), *Hydrothermal Vents and Processes.* Geol. Soc. Spec. Publ. London, 87:207–222.

Lein, A.Y., Ul'yanova, N.V., Grinenko, V.A., Bibikova, Y.V., and Lisitsyn, A.P., 1993. Mineralogical and geochemical features of the Manus Basin hydrothermal sulfide ores, Bismark Sea. *Geochem. Int.,* 30:57–71.

Marchig, V., Puchelt, H., Rosch, H., and Blum, N., 1990. Massive sulfides from ultra-fast spreading Ridge, East Pacific Rise at 18–21°S: a geochemical stock report. *Mar. Min.,* 9:459–493.

Mills, R.A., 1995. Hydrothermal deposits and metalliferous sediments from TAG, 26°N Mid-Atlantic ridge. *In* Parson, L.M., Walker, C.L., and Dixon, D.R. (Eds.), *Hydrothermal Vents and Processes.* Geol. Soc. Spec. Publ. London, 87:121–132.

Ohmoto, H., 1986. Stable isotope geochemistry of ore deposits. *In* Valley, J.W., Taylor, H.P., Jr., and O'Neil, J.R. (Eds.), *Stable Isotopes in High Temperature Geological Processes.* Miner. Soc. Amer., Rev. Mineral., 16:491–559.

Ohmoto, H., and Rye, R.O., 1979. Isotopes of sulfur and carbon. *In* Barnes, H.L. (Ed.), *Geochemistry of Hydrothermal Ore Deposits* (2nd ed.): New York (Wiley), 509–567.

Rees, C.E., Jenkins, W.J., and Monster, J., 1978. The sulphur isotopic composition of ocean water sulphate. *Geochim. Cosmochim. Acta,* 42:377–381.

Rona, P.A., Hannington, M.D., Raman, C.V., Thompson, G., Tivey, M.K., Humphris, S.E., Lalou, C., and Petersen, S., 1993. Active and relict seafloor hydrothermal mineralization at the TAG hydrothermal field, Mid-Atlantic Ridge. *Econ. Geol.,* 88:1987–2013.

Rona, P.A., McGregor, B.A., Betzer, P.R., Bolger, G.W., and Krause, D.C., 1975. Anomalous water temperatures over Mid-Atlantic Ridge Crest at 26°N. *Deep-Sea Res. Part A,* 22:611–618.

Rona, P.A., Thompson, G., Mottl, M.J., Karson, J.A., Jenkins, W.J., Graham, D., Mallette, M., Von Damm, K., and Edmond, J.M., 1984. Hydrothermal activity at the TAG hydrothermal field, Mid-Atlantic Ridge crest at 26°N. *J. Geophys. Res.,* 89:11365–11377.

Rye, R.O., Roberts, R.J., Snyder, W.S., LaHusen, G.L., and Motica, J.E., 1984. Textural and stable isotope studies of the Big Mike cupriferous volcanogenic massive sulfide deposit, Pershing County, Nevada. *Econ. Geol.,* 79:124–140.

Sakai, H., Des Marais, D.J., Ueda, A., and Moore, J.G., 1984. Concentrations and isotope ratios of carbon, nitrogen and sulfur in ocean-floor basalts. *Geochim. Cosmochim. Acta,* 48:2433–2441.

Sangster, D.F., 1968. Relative sulfur-isotope abundances of ancient seas and stratabound sulfide deposits. *Proc. Geol. Assoc. Can.,* 17:79–91.

Seccombe, P.K,. and Clark, G.S., 1981. Sulfur isotope and element variations in the South Bay mine, northwestern Ontario. *Econ. Geol.,* 76:621–636.

Seccombe, P.K., Godwin, C.I., Krouse, H.R., and Juras, S.J., 1990. Sulphur and lead isotope studies of the Buttle Lake massive sulphide deposits, Vancouver Island, B.C., Canada: sources of ore constituents in a submarine exhalative environment. *AusIMM Proc. Pacific Rim Conf.,* 2:419–426.

Shanks, W.C., III, Bischoff, J.L., and Rosenbauer, R.J., 1981. Seawater sulfate reduction and sulfur isotope fractionation in basaltic systems: interaction of seawater with fayalite and magnetite at 200-350°C. *Geochim. Cosmochim. Acta,* 45:1977–1995.

Shanks, W.C., III., Böhlke, J.K., Seal, R.R., II, 1995. Stable isotopes in mid-ocean ridge hydrothermal systems: interactions between fluids, minerals, and organisms. *In* Humphris, S.E., Zierenberg, R.A., Mullineaux, L.S., Thompson, R.E. (Eds.), *Seafloor Hydrothermal Systems: Physical, Chemical, Biological, and Geological Interactions.* Geophys. Monogr., 91:194–221.

Shanks, W.C., III, and Seyfried, W.E., Jr., 1987. Stable isotope studies of vent fluids and chimney minerals, southern Juan de Fuca Ridge: sodium metasomatism and seawater sulfate reduction. *J. Geophys. Res.,* 92:11387–11399.

Solomon, M., Eastoe, C.J., Walshe, J.L., and Green, G.R., 1988. Mineral deposits and sulfur-isotope abundances in the Mount Read Volcanics between Que River and Mt Darwin, Tasmania. *Econ. Geol.,* 83:1307–1328.

Spooner, E.T.C., 1977. Hydrodynamic model for the origin of the ophiolitic cuperiferous pyrite ore deposits of Cyprus. *Geol. Soc. Spec. Publ. London,* 7:58–71.

Styrt, M.M., Brackmann, A.J., Holland, H.D., Clark, B., Pisutha-Arnond, V., Eldridge, C.S., and Ohmoto, H., 1981. The mineralogy and isotopic composition of sulfur in hydrothermal sulfide/sulfate deposits on the East Pacific Rise, 21°N latitude. *Earth Planet. Sci. Lett.,* 53:382–390.

Taylor, B.E., 1987. Stable isotope geochemistry of ore-forming fluids. *Mineral. Assoc. Can., Short Course,* 13:337–445.

Thompson, G., Mottl, M.J., and Rona, P.A., 1985. Morphology, mineralogy and chemistry of the hydrothermal deposits from TAG area, 26°N, Mid-Atlantic Ridge. *Chem. Geol.,* 49:243–257.

Tivey, M., Humphris, S.E., Thompson, G., Hannington, M.D., and Rona, P.A., 1995. Deducing patterns of fluid flow and mixing within the TAG active hydrothermal mound using mineralogical and geochemical data. *J. Geophys. Res.,* 100:12527–12555.

Woodruff, L.G., and Shanks, W.C., 1988. Sulfur isotope study of chimney minerals and hydrothermal fluids from 21°N, East Pacific Rise: hydrothermal sulfur sources and disequilibrium sulfate reduction. *J. Geophys. Res.,* 93:4562–4572.

Date of initial receipt: 5 June 1996
Date of acceptance: 1 April 1997
Ms 158SR-206

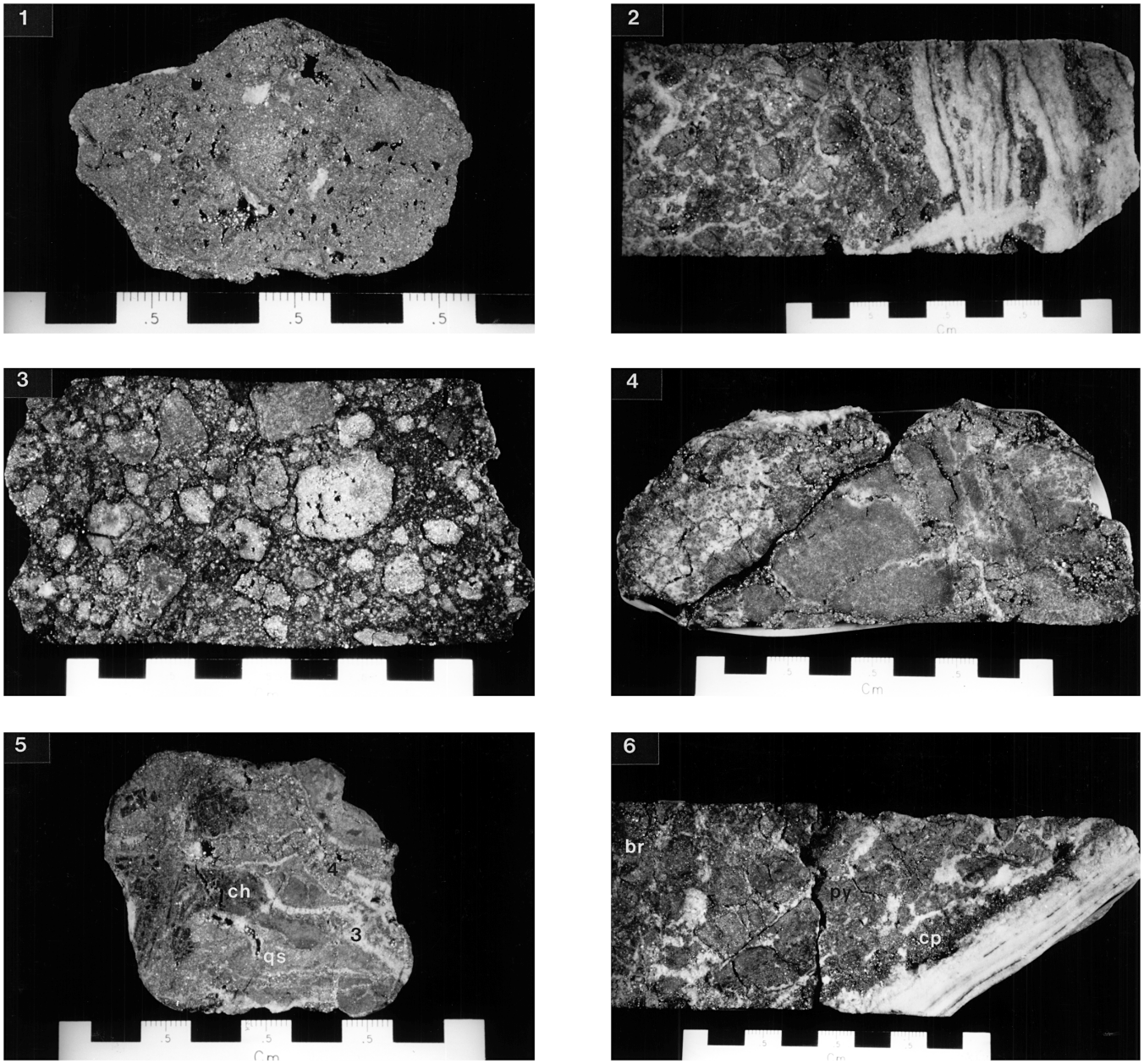

Plate 1. **1.** Massive sulfide. Massive, granular pyrite with interstitial anhydrite. Black areas are pore space. Sample 158-957G-1N-1, Piece 3, 10–15 cm. Scale bar in cm. **2.** Pyrite-anhydrite breccia with Stage 5 anhydrite vein. Rounded to subangular clasts of pyrite ± chalcopyrite set in a matrix of anhydrite. Vein consists of crustiform anhydrite with bands and clots of pyrite and chalcopyrite. Sample 158-957C-7N-3, Piece 4A, 28–50 cm. Scale bar in cm. **3.** Pyrite-silica breccia. Subrounded to angular clasts of pyrite and pyrite-quartz set in a fine-grained quartz with disseminated pyrite matrix. Sample 158-957H-5N-1, Piece 5A, 28–40 cm. Scale bar in cm. **4.** Silicified wallrock breccia. Silicified, sericitized, and pyritized basalt cut by quartz-pyrite-chalcopyrite stockwork (Stage 2 veins). Sample 158-957c-16N-2, Pieces 7A and 7B, 67–82 cm. Scale bar in cm. **5.** Chloritized basalt breccia. Basalt that has been initially chloritized (ch) and then overprinted by quartz-sericite alteration (qs). Quartz-only Stage 3 (3) and Stage 4 pyrite-quartz (4) veins through sample. Sample 158-957E-17R-1, Piece 7, 39–44 cm. Scale bar in cm. **6.** Stage 5 anhydrite vein (as illustrated in Fig. 6). Vein consists of fine-grained crustiform banded anhydrite with a 0.5- to 1.5-cm-thick chalcopyrite selvage (cp). A pyritization halo (py) extends 4 cm into the pyrite-silica breccia (br). Sample 158-957C-13N-2, Pieces 3A and 3B, 15–30 cm. Scale bar in cm.

Prior Chapter Contents Next Chapter